

Supplementary Information

Microkinetic Insights into the role of Catalyst and Water Activity on the Nucleation, Growth, and Dissolution during COF-5 Synthesis

Anish V. Dighe^{1,‡}, Rajan R. Bhawnani^{1,‡}, Prem K.R. Podupu¹, Naveen Dandu^{1,2}, Anh Ngo^{1,2}, Santanu Chaudhuri^{1,2}, and Meenesh R. Singh^{1,*}

¹Department of Chemical Engineering, University of Illinois at Chicago, Chicago, IL 60607, United States

²Argonne National Laboratory, Lemont, IL 60439

[‡]Authors contributed equally

***Corresponding Author:**

Prof. Meenesh R. Singh
Assistant Professor
Department of Chemical Engineering
929 W. Taylor St
University of Illinois at Chicago
Chicago, IL 60607
Tel: (312) 996-3424
Email: mrsingh@uic.edu

Keywords: Covalent Organic Frameworks, COF-5, Catalysis, Oriented Attachment, Microkinetic Modeling

Section S1: Experimental synthesis and characterization

S1.1 Materials and Method

2,3,6,7,10,11-hexahydroxytriphenylene was purchased from TCI America (>95% purity), and 1,4-phenylene bis boronic acid (PBBA) was purchased from Matrix Scientific (98% purity). Solvents and catalysts were purchased from Millipore Sigma and were used without any further purification (maximum purity as obtained i.e >98%). 60 mg of 2,3,6,7,10,11-hexahydroxytriphenylene (HHTP) and 40 mg of Phenyl bis-boronic acid (PBBA) were dissolved in 30 mL of 4:1 v/v mixture of 1,4-dioxane and toluene resulting in 8mM and 12mM concentration of HHTP and PBBA respectively. The mixture was sonicated for 2 minutes to ensure complete dissolution and was filtered with a 0.45 μm Polytetrafluoroethylene (PTFE) filter to eliminate any particulate impurities. An amount of 5 molar equivalent to HHTP, i.e., 40mM of catalyst (formic acid, acetic acid, phenol, methanol), was added to this mixture. 1 mL of this bulk solution was aliquoted in the batch cell fixed on top of the ATR-FTIR setup, as shown in **Figure S1**. The temperature-controlled ATR ZnSe plate was heated to the desired temperature, and the spectra were recorded in-situ. For ex-situ XRD analysis, separate experiments were performed to prepare samples in bulk for powder XRD analysis. The synthesized suspension was separated using 0.22 μm Polytetrafluoroethylene (PTFE) filter in an autovial. This powder was washed thoroughly with acetone and was dried under vacuum for 24 hours prior to performing p-XRD.

S1.2 Characterization

In-situ FT-IR measurements

In-situ FT-IR experiments were performed using a Bruker Invenio-S Spectrometer in ATR mode with the help of a temperature-controlled ZnSe plate (**Figure S1**). The batch cell mounted on top of the plate (as shown in **Figure S1**) was 3D printed in-house. The procedure was repeated three times for each experimental condition to ensure reproducibility of the obtained yield.

For calibrations, known amounts of COF-5 powder were dissolved in 5mL acetone each, and the spectra were recorded at different concentrations using the same setup.

X-ray diffraction measurements

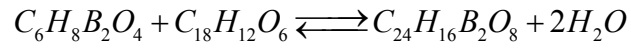
High-resolution X-Ray diffraction measurements were performed on a Bruker-Nano Discover 8 X-Ray Diffraction system. The system uses Cu as the target material, with $\text{CuK}\alpha$ radiation $\lambda=1.54\text{\AA}$. The generator was set to 40kV and 40mA. The resolution for measurements was set to $2\theta=0.02^\circ$.

BET surface area and pore size distribution measurements

N_2 adsorption isotherms were carried out by means of a Micrometrics Tristar II 3020 at 77K. The BET surface area was determined in the P/P_0 range of 0.0 to 1.0. **Figure S16** shows the adsorption and the desorption isotherm plots.

Section S2: Calculation of Molecular weight of the smallest SBU (initiation reaction)

The formation of the smallest SBU is shown as follows:



Applying mass balance to the above equation:

MW of SBU = (MW of PBBA) + (MW of HHTP) – (MW of 2 water molecules)

MW of SBU = (165.75) + (324.29) – (2 x 18)

MW of SBU = 454.04 g mol⁻¹

Section S3: Density Functional Theory (DFT) calculations:

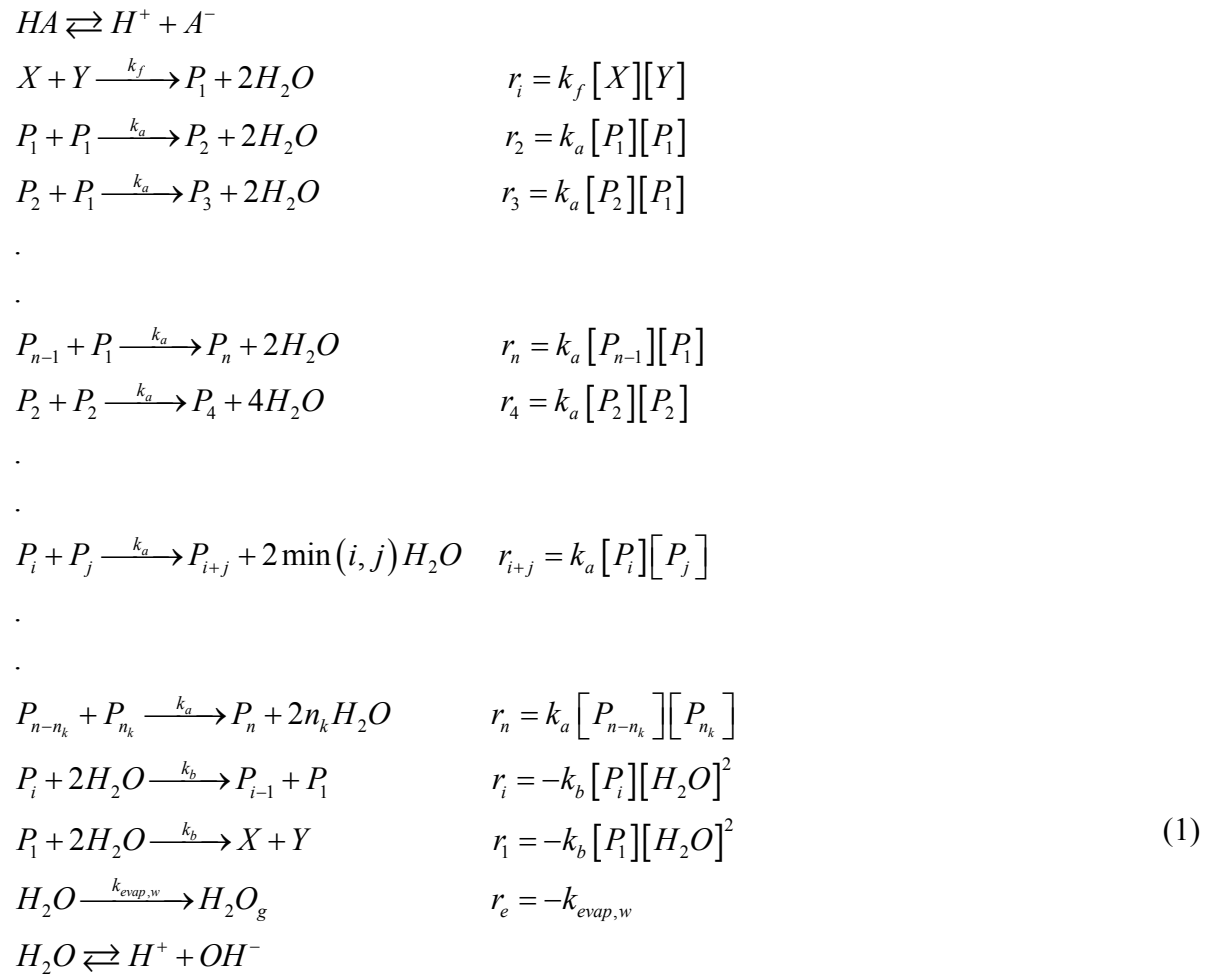
We considered the boron ester bond formation reaction between HHTP and PBBA, as shown in **Figure S4**. Geometry optimizations of reactants were performed under the density functional theory approach implemented on Gaussian 16 software package (1) using ω -B97Xd functional (2) and 6-31G** basis set.(3) The transition state optimizations were performed using quadratic synchronous transit – 3 (QST3) (4, 5) approach to obtain an efficiently converged transition state structure. This approach resulted in one imaginary frequency whose eigenvectors were directed towards reactants/products, confirming the right configuration of the transition state structure. Later, we performed an Intrinsic Reaction Coordinate (IRC) (6) scan to confirm the righteousness of the reaction pathway between the transition state and the reactants/products (**Figure S5**). Additionally, the conductor-like polarizable continuum model (CPCM) model was used to account for calculations in the presence of 1,4-dioxane as solvent. All the calculations were performed at 90°C to obtain free energy values at that temperature.

Boronic ester bond formation with and without catalysts is considered to study their effect on the reduction of transition state energy barriers. Water, methanol, phenol, acetic acid, and formic acid are considered catalysts. The relaxed geometries of reactants and transition state structures are shown in **Table S1**. In each case, transition state energy barriers, Gibbs free energy difference between reactants and transition states, were calculated. Our calculations suggest that the lower the pKa of the catalyst, the lower is the activation energy barrier, complementing experimental observations, except in the case of phenol. We anticipate that the steric effect of the benzene ring of phenol might be the reason for the slight increase in the activation energy barrier.

Section S4: Computational Details

S4.1 Microkinetic Model

The reaction scheme and the corresponding microkinetic rate equations are shown in equation (1). The reaction proceeds with the formation of the smallest secondary building unit (SBU), which undergoes chain addition to form higher-order growth units. The SBUs smaller than the energetically stable size of COF-5 undergoes step reaction. The energetically stable size is the smallest observed size of the COF-5 crystal in the literature and is found to be 12 nm.(7) The chain and step addition of COF-5 follows Flory's approximation(8) such that a single value of rate constant minimizes the error with experimental data, as shown in the error minimization section. The formation of COF-5 is catalyzed due to the protonation of the hydroxyl group and results in the release of water.(9) The dissociation of acid and water is assumed to be in equilibrium. At any time, the concentration of reactants is calculated using a mass balance constraint. The evaporation equations are also provided if needed to be considered. Electroneutrality was enforced to balance the total charge in the reaction scheme. The "ode45" solver in MATLAB was used to solve the system of equations. The equations are as follows:



Where reactant X represents PBBA, reactant Y represents HHTP. The square brackets denote the concentration in mol/L. $[P_i]$ is the concentration of SBU of size $i = 1, 2, \dots, n - n_k$. n is the largest size of crystal formed by the addition of SBUs considered in the model. n_k is the smallest energetically stable size of SBU. $j = 1, 2, \dots, n_k$ represents the SBU sizes smaller than energetically stable SBU, which undergo aggregation to form higher-order SBUs. $[HA]$ is the concentration of acid-catalyst used in the experiments and $[H_2O]$ is the concentration of water in the system. The initiation reaction is the formation of the smallest SBU, which has a forward rate constant k_f . The rate constants for chain and step additions are equal based on Flory's approximation and are represented by k_a . The rate constant for hydrolysis reaction due to accumulation of water in the system is given by k_b . The algebraic equations which enforce mass balance and electroneutrality of the system are given below. $k_{evap,w}$ is the rate constant for evaporation of water. Subscript h denotes any size of SBU between 1 and n , while subscripts i and j obey the bounds given above. The dissociation of H_2O and HA is assumed to be faster than the initiation reaction of COF-5 such that H_2O and HA are in equilibrium with their respective dissociated species. Units of rate constants are given in table S2.

Mass balance constraint:

$$X_{moles} = X_{0,moles} - P_{1,tot,moles} \quad (2)$$

$$Y_{moles} = Y_{0,moles} - P_{1,tot,moles} \quad (3)$$

$$[X] = \frac{X_{moles}}{V} \quad (4)$$

$$[Y] = \frac{Y_{moles}}{V} \quad (5)$$

Where, subscript 0 represents initial value, *tot* represents total, and *moles* represents a quantity in moles, V (L) is the volume at that time.

Electroneutrality:

$$[H^+] = [OH^-] + [A^-] \quad (6)$$

Catalyst effect on rate constant:

$$k_f = k'_f \left(1 - \gamma \log([H^+]) \right) \quad (7)$$

Where, k_f' is the forward rate of reaction without catalysis. $(1 - \gamma \log([H^+]))$ is the dimensionless factor which dictates the effect of catalysis on the forward rate constant. γ (dimensionless) is the volume of active catalytic sites per unit concentration.

Acid and water dissociation to calculate the concentration of proton:

$$\frac{[H^+][A^-]}{[HA]_0 - [A^-]} = K_a \quad (8)$$

$$\frac{[H^+][OH^-]}{[H_2O]} = K_w \quad (9)$$

Substitute equations (6) and (8) in (9) to obtain:

$$[H^+]^3 + K_a [H^+]^2 - (K_a [HA]_0 + K_w [H_2O])[H^+] - K_w K_a [H_2O] = 0 \quad (10)$$

The positive root of equation (8) is the concentration of proton in the solution. The dissociation constant of acid (K_a) was assumed to not vary significantly as a function of temperature. However, the temperature dependence of dissociation constant of water (K_w) was implemented as follows(10):

$$\log(K_w) = 12 \left(\log(1+Z) - \frac{Z\rho_{H_2O}}{Z+1} \left(0.642044 - \frac{56.8534}{T} - 0.375754\rho_{H_2O} \right) \right) + pK_w^G + 2 \log\left(\frac{M_w}{1000}\right) \quad (11)$$

$$Z = \rho_{H_2O} \exp\left(-0.864671 + \frac{8659.19}{T} - \frac{22786.2}{T^2} \rho_{H_2O}^{\frac{2}{3}}\right) \quad (12)$$

$$pK_w^G = 0.61425 + \frac{48251.33}{T} - \frac{67707.93}{T^2} + \frac{10102100}{T^3} \quad (13)$$

Where, T (K) is the temperature, M_w (g/mol) is the molecular weight of water, ρ_{H_2O} (g/cc) is the density of water.

$$k_{evap} = 1.703 \times 10^{-7} \exp\left(167.8135 \left(\frac{1}{273.15 + 90} - \frac{1}{273.15 + T} \right) \right) \quad (14)$$

The temperature of the reaction mixture at any time is calculated in the experiments.

The complete set of rate equations can now be obtained.

The rate of change in the concentration of P_i due to forwarding reactions involving P_j is given below:

$$\left. \frac{d[P_i]}{dt} \right|_j = \begin{cases} r_i - k_a [P_i] \sum_{l=i}^{n-i} P_l & \text{if } i = j \\ -k_a [P_i] [P_j] & \text{if } i < 2j, j \neq i \\ -k_a [P_i] ([P_j] - [P_{j-i}]) & \text{if } i > 2j, i + j \leq n \\ k_a [P_i] [P_{j-1}] & \text{if } i > 2j, i + j > n \end{cases} \quad (15)$$

$$\text{Where, } r_i = \begin{cases} k_f [X][Y] & \text{if } i = j = 1 \\ 0 & \text{otherwise} \end{cases}$$

The rate of change in the concentration of P_h due to hydrolysis reaction is given below:

$$\left. \frac{d[P_h]}{dt} \right|_b = \begin{cases} k_b [H_2O]^2 \left(\sum_{l=2}^n [P_l] - [P_1] \right) & \text{if } h = 1 \\ -k_b [H_2O]^2 [P_h] & \text{if } h > 1 \end{cases} \quad (16)$$

The change in the concentration of water due to forward reactions of any P_h is given by:

$$\left. \frac{d[H_2O]}{dt} \right|_h = \begin{cases} 2k_f [X][Y] + 2w_p k_a [P_h] \sum_{l=i}^{n-i} [P_l] & \text{if } h = 1 \\ 2w_p k_a [P_h] \sum_{l=h}^{n-h} [P_l] & \text{if } h > 1 \end{cases} \quad (17)$$

Where, w_p is $\min(h, l)$. The change in the concentration of water due to hydrolysis reaction is given by:

$$\left. \frac{d[H_2O]}{dt} \right|_b = -2k_b [H_2O]^2 \sum_{l=1}^n [P_l] \quad (18)$$

The rate of change of water concentration due to evaporation is given by:

$$\left. \frac{d[H_2O]}{dt} \right|_e = -k_{evap,w} \quad (19)$$

The total rate of change of concentration of P_i is:

$$\frac{d[P_i]}{dt} = \sum_{j=1}^{n_k} \left. \frac{d[P_i]}{dt} \right|_j + \left. \frac{d[P_i]}{dt} \right|_b \quad (20)$$

The total rate of change of concentration of water due to all P_h is:

$$\frac{d[H_2O]}{dt} = \sum_{h=1}^n \left. \frac{d[H_2O]}{dt} \right|_h + \left. \frac{d[H_2O]}{dt} \right|_b + \left. \frac{d[H_2O]}{dt} \right|_e \quad (21)$$

All of the concentration values are obtained by calculating moles at each time step and then dividing the moles by volume (V) at that time. For the rate equations, volume contribution is added to the net rate of the components. The equations are as follows.

$$[P_i] = \frac{n_i}{V} \quad (22)$$

$$\frac{1}{V} \frac{dn_i}{dt} = \text{net rate} + \frac{[P_i]}{V} \frac{dV}{dt} \quad (23)$$

Net rate is the RHS of equation (20).

A similar relationship with volume was used for water concentration as well.

S4.2 Post-analysis of Solution of Microkinetic Model

S4.2.1 Calculation of Crystalline Fraction

Since the experimental analysis was performed ex-situ, only the concentration of SBUs higher than the smallest energetically stable size was considered. The total concentration of the smallest SBU is used to calculate the yield of the reaction.

$$[P_1]_{tot} = \sum_{h=n_k}^n h [P_h] \quad (24)$$

The crystalline fraction is the total concentration of the smallest SBU divided by the concentration of the limiting reactant.

$$c_f = \frac{[P_1]_{tot}}{\min([X], [Y])} \quad (25)$$

S4.2.2 Calculation of Grain Size

The number of smallest SBUs in a single lattice of COF-5 is two. Hence the volume per number of smallest SBU is given as:

$$v_{SBU} = \frac{2}{\rho_{lattice}} \quad (26)$$

v_{SBU} (\AA^3) is the volume per SBU. $\rho_{lattice}$ (\AA^3) is the volume of unit cell (lattice) of COF-5.

$$\rho_{lattice} = a^2 c \sin(60^\circ) \quad (27)$$

$a = 30.0198 \text{ \AA}$ and $c = 3.404 \text{ \AA}$ are the lattice parameters of COF-5.

The average size of the crystal formed is calculated as follows:

$$\langle h \rangle = \frac{[P_1]_{tot}}{\sum_{h=n_k}^n [P_h]} \quad (28)$$

The volume of the crystal V_{cryst} (\AA^3) formed due to average size is:

$$V_{cryst} = \frac{\langle h \rangle}{v_{SBU}} \quad (29)$$

$$V_{cryst} = d_1^2 d_2 \sin(60^\circ) \quad (30)$$

d_1 (\AA), and d_2 (\AA) are linearly dependent, and the ratio is based on the lattice parameters to enforce the shape of the crystal detected in the XRD.

$$d_2 = \frac{c}{a} d_1 \quad (31)$$

Substitute equations (26), (28), (30), and (31) in equation (29) and solve for d_2 .

The average grain size g_s (\AA) from the model is then

$$g_s = \frac{d_1 + d_2}{2} \quad (32)$$

Section S5: Optimization of Values of the Parameters in the Microkinetic Model

Step 1: Optimize k_f

- Set $k_b, k_a = 0$.
- Assume no water accumulation, hence: $\frac{d[H_2O]}{dt} = 0$.
- Optimize k_f such that it minimizes the error between theoretically calculated c_f and the experimentally calculated normalized yield.
- The experimentally calculated yield represents the yield of COF-5 when the reaction mixture is open to the atmosphere.

Step 3: Optimize k_a

- Set $k_b = 0$ and use the optimized value of k_f from the previous step.
- Assume no water accumulation, hence: $\frac{d[H_2O]}{dt} = 0$.
- Optimize k_a such that it minimizes the error between theoretically calculated g_s and the experimental grain size from XRD.

Step 3: Optimize k_b

- Use optimized values of k_f and k_a from previous steps.
- Assume no water evaporation, hence: $\left. \frac{d[H_2O]}{dt} \right|_e = 0$.
- Optimize k_b such that it minimizes the error between theoretically calculated c_f and the experimentally calculated normalized yield.
- The experimentally calculated yield represents the yield of COF-5 when the reaction mixture is closed.

Step 4: Optimize $k_{evap,w}$

- Use optimized values of k_f, k_b, k_a from previous steps.
- Optimize $k_{evap,w}$ such that it minimizes the error between theoretically calculated c_f and the experimentally calculated normalized yield.
- The experimentally calculated yield represents the yield of COF-5 when the reaction mixture is open to the atmosphere.

Step 5: Calculate γ :

- Find optimum k_f values for two different catalysts at a constant temperature.

- Calculate γ from equation (7) such that k'_f for both catalysts at that temperature is equal.

The rate constant values only need to error minimized against experimental data at two different temperatures for the same catalyst. Rate constants at any other temperature are calculated using the Arrhenius relationship.

Section S6: Rate Calculations

(1) Rate of initiation:

$$r_i = k_f [X][Y] \quad (33)$$

(2) Rate of chain addition:

$$r_c = k_a [P_1] \sum_{h=1}^{n_k-1} [P_h] \quad (34)$$

(3) Rate of step growth:

$$r_s = k_a \sum_{j=2}^{n_k} \sum_{i=2}^{n_k-j} [P_i][P_j] \quad (35)$$

(4) Termination:

$$r_t = k_a \sum_{j=n_k+1}^n \sum_{i=2}^{n-j} [P_i][P_j] \quad (36)$$

(5) Rate of hydrolysis reaction of SBUs (using equation (17)):

$$r_b = \sum_{h=1}^n \left. \frac{d[P_h]}{dt} \right|_b \quad (37)$$

Volumetric rates are calculated by calculating change in the concentration of $[P_1]_{tot}$ due to any of the reactions listed above.

Section S7: Calculation of Dominant Pathway Using Reaction Network

The reaction network presented in Section S4 can be represented as a reaction network where every SBU (P_i) is a node, and the reaction that forms the node is an edge connecting the two nodes. For the reactions considered in this study, the reaction network results in 20,000 nodes and over 10 million edges. The most dominant pathway that forms the smallest energetically stable crystal size (P_{750}) can be calculated such that sum of the rates of reactions that form P_{750} is minimum. The results of these calculations are shown in **Figure S11**. In all subplots of **Figure S11**, the nodes are represented with a colored line. The color of the node represents the number of reactions (edges) emerging from the node (out-degree). All edges except those representing the most dominant pathway are hidden. The edge thickness represents the rate of the reaction relative to the highest rate of the reaction observed in all of the simulated experimental conditions. The reaction network is time-dependent such that changes in the rate of reactions affect the reaction network. Hence, the reaction network at the time of nucleation onset is presented to elucidate the dynamics of the formation of the smallest energetically stable nuclei.

Section S8: PXRD Characterization

The powdered samples collected at different times were analyzed using powdered X-Ray diffraction using a Bruker D8 Discover X-ray diffraction system. The spectra were recorded using Cu K- α radiation, and the grain size from the obtained spectra was calculated using Scherrer's equation:

$$g_{s,e} = \frac{K\lambda}{\beta \cos(\theta)} \quad (38)$$

where,

$g_{s,e}$ is the average grain size,

$K = 0.9394$ is the shape factor,

λ is the wavelength of radiation (=1.54 Å for Cu K- α radiation),

β is the full-width half maximum of the peaks from the spectra (in radians),

θ is the Bragg angle corresponding to (100) Miller plane.

Section S9: Calculation of Nucleation and Growth Kernels

The estimated nucleation and growth kernels are given below.

$$N(\xi, T) = k_{0,n} \xi^{A_n} (1 - \xi)^{B_n} \exp\left(-\frac{\Delta E_{a,n}}{RT}\right) \quad (39)$$

Where, N (s^{-1}) is the nucleation rate, $k_{0,n}$ (s^{-1}) is the pre-exponential factor, ξ is the reaction extent, A_n is the order of the product phase (reaction extent), B_n is the order of the reactant phase (limiting reactant), $\Delta E_{a,n}$ (J/mol) is the activation barrier for nucleation, R (J/(mol K)) is the gas constant, and T (K) is the temperature.

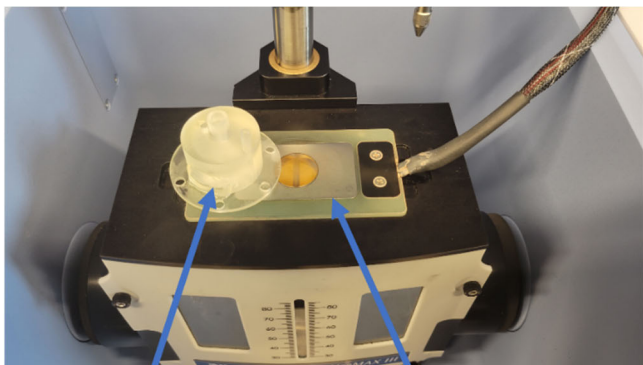
$$G(\xi, T) = k_{0,g} \xi^{A_g} (1 - \xi)^{B_g} \exp\left(-\frac{\Delta E_{a,g}}{RT}\right) \quad (40)$$

Where, G ($m s^{-1}$) is the growth rate, $k_{0,g}$ ($m s^{-1}$) is the pre-exponential factor, ξ is the reaction extent, A_g is the order of the product phase (reaction extent), B_g is the order of the reactant phase (limiting reactant), $\Delta E_{a,g}$ (J/mol) is the activation barrier for growth, R (J/(mol K)) is the gas constant, and T (K) is the temperature.

Section S10: Integrated Rate Law

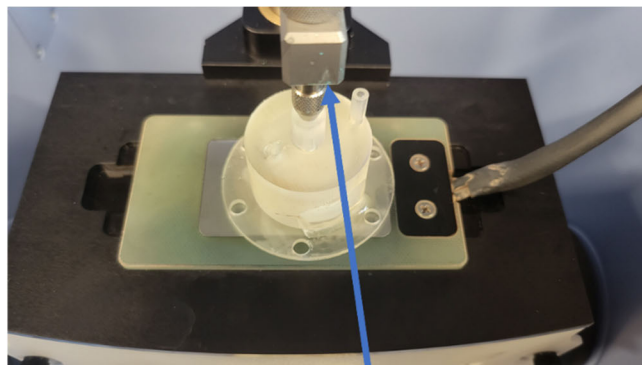
$$\frac{1}{[X]_0 - [Y]_0} \ln \frac{[X][Y]_0}{[Y][X]_0} = k_{f,expt} t \quad (41)$$

Where, $k_{f,expt}$ is the rate constant of initiation reaction obtained from experiments, t is time, and other variable names and terminologies are same as given in Section S4.



In-house 3D printed
batch cell

Temperature
controlled plate
with ZnSe crystal



Steel clamp to fix
the cell on top of
the crystal

Figure S1: In-situ temperature-controlled ATR-FTIR setup with in-house 3D printed batch cell.

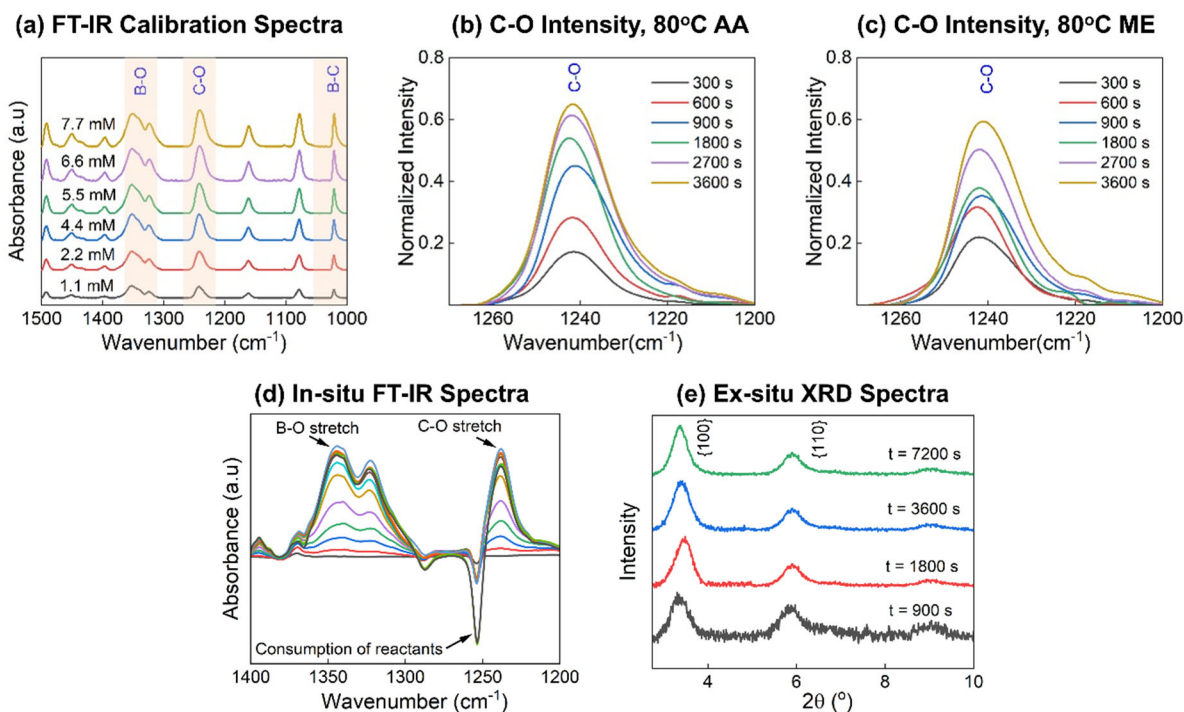


Figure S2: FT-IR characterization of COF-5 synthesis. (a) Complete FTIR spectra of COF-5 powder at known concentrations of SBU₁ calculated using the weight of COF-5 powder. The bonds which are formed during the formation of COF-5 and their locations are highlighted. (b) An increase in the normalized intensity of C-O peaks as a function of time at the synthesis temperature of 80° C and acetic acid as the catalyst. (c) An increase in the normalized intensity of C-O peaks as a function of time at the synthesis temperature of 80° C and methanol as the catalyst. (d) The spectra obtained from in-situ FT-IR analysis at 800C and 4:1 (v/v) dioxane : toluene conditions, show an increase in the absorbance intensity of Boron-Oxygen (B-O) and Carbon-Oxygen (C-O) bond stretches due to the formation of COF-5 growth units. The bonds that are unique to the reactants show negative absorbance intensity denoting consumption of reactants. (e) The XRD spectra show an increase in the grain size of COF-5 crystals as time increases.

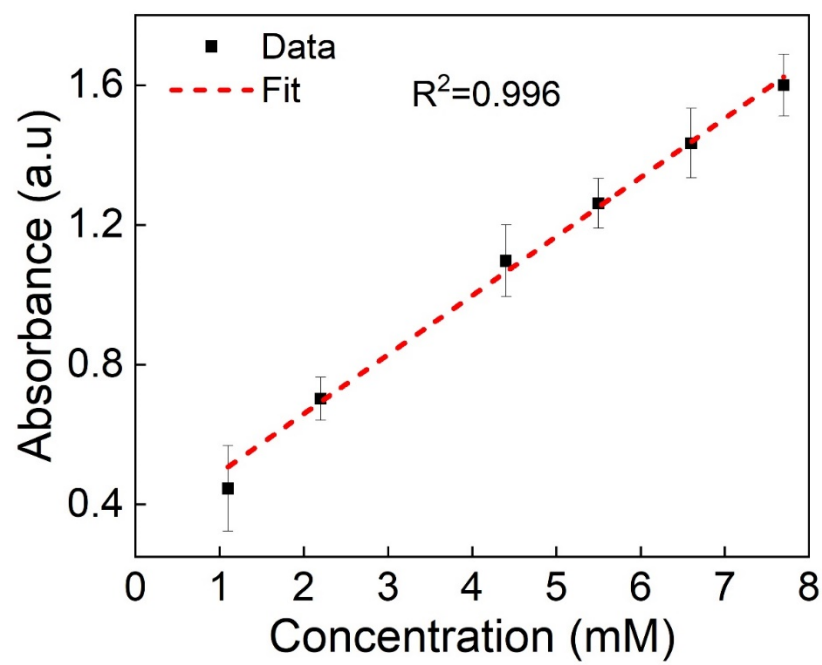


Figure S3: Calibration curve obtained using C-O bond intensity at 1241cm^{-1} .

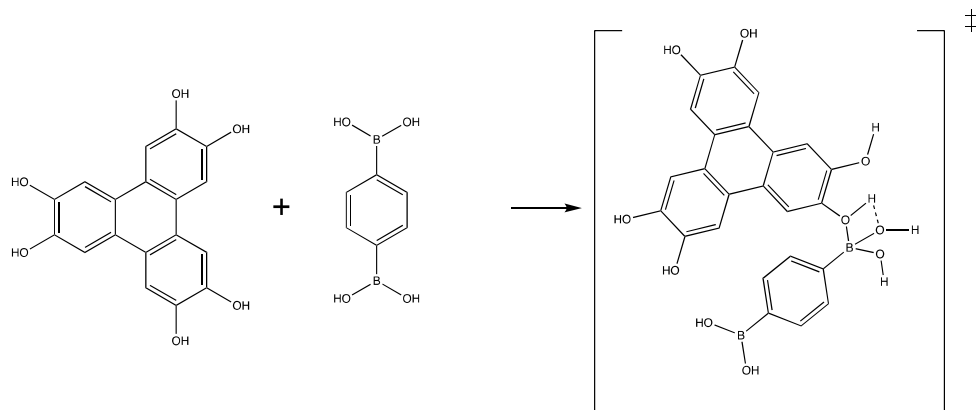


Figure S4: Boronic ester bond formation (transition state) between HHTP and PBBA without catalyst.

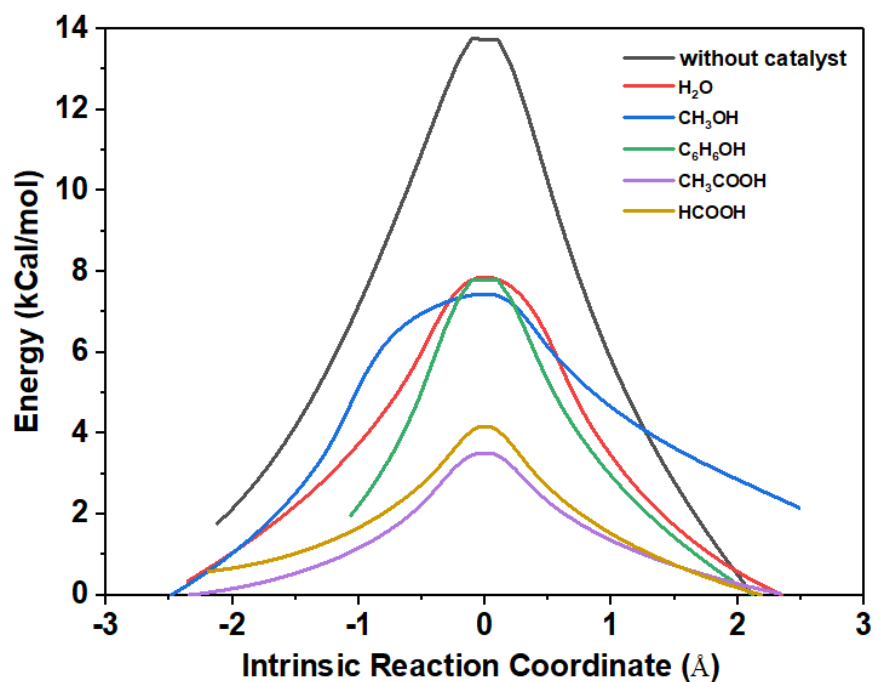


Figure S5: Intrinsic Reaction Coordinate reaction pathway for the reaction between HHTP and PBBA with and without catalyst. Note: the reactants and products in IRC method are not relaxed structures (only approximate structures).

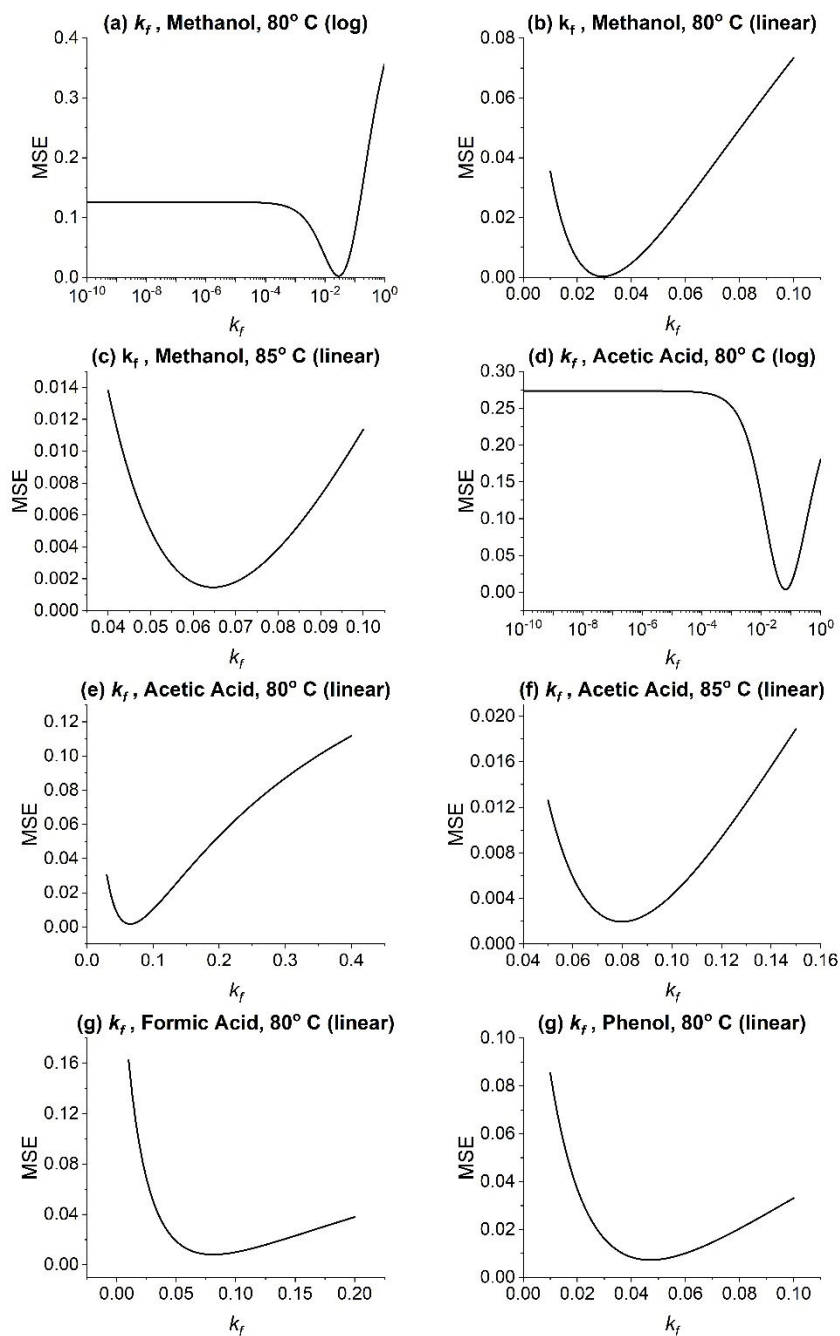


Figure S6: Parameter scan for error minimization against experimental data for the forward rate constant of the microkinetic model.

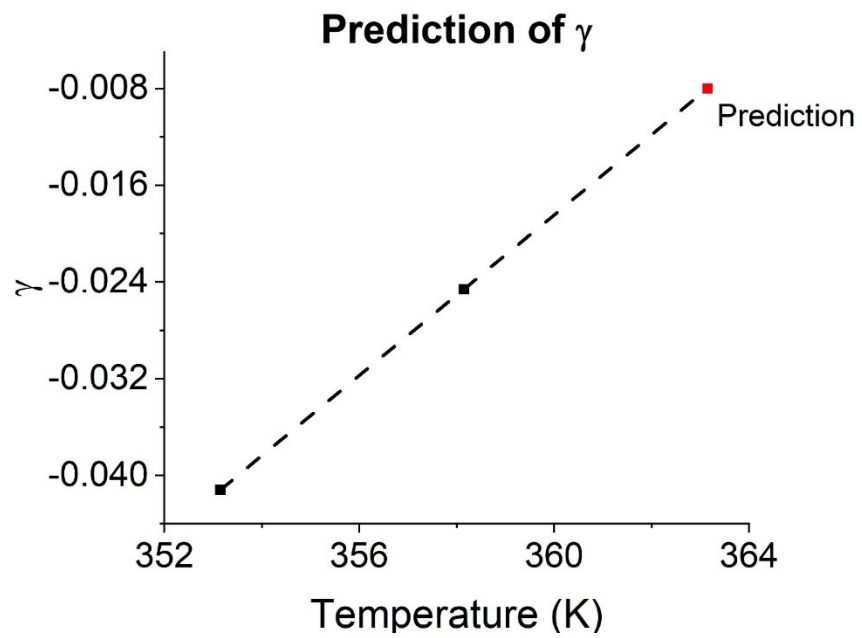


Figure S7: Prediction of γ

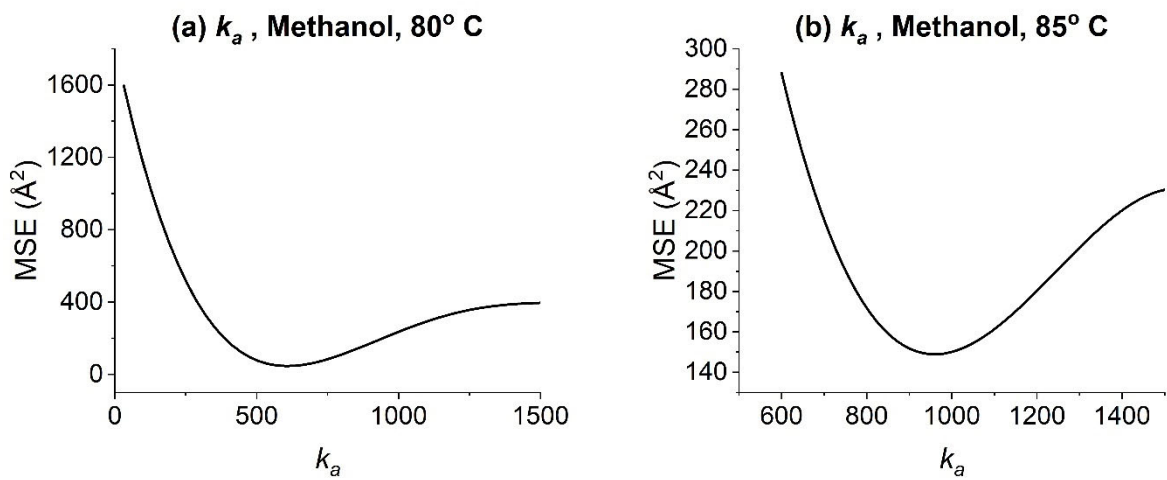


Figure S8: Parameter scan for error minimization against experimental data for the aggregation rate constants involved in the microkinetic model.

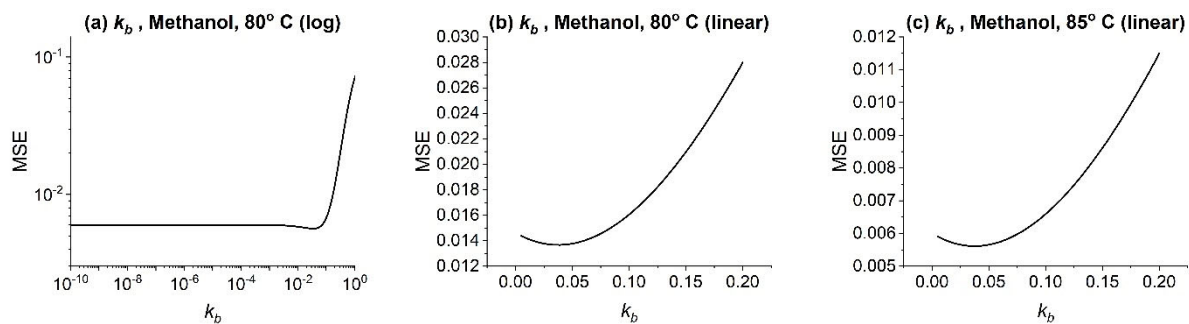


Figure S9: Parameter scan for error minimization against experimental data for the backward rate constants involved in the microkinetic model.

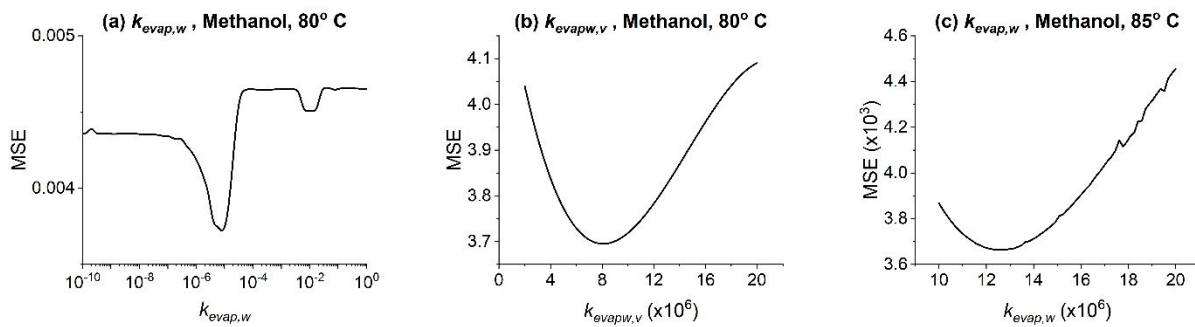


Figure S10: Parameter scan for error minimization against experimental data for the water evaporation rate constants involved in the microkinetic model.

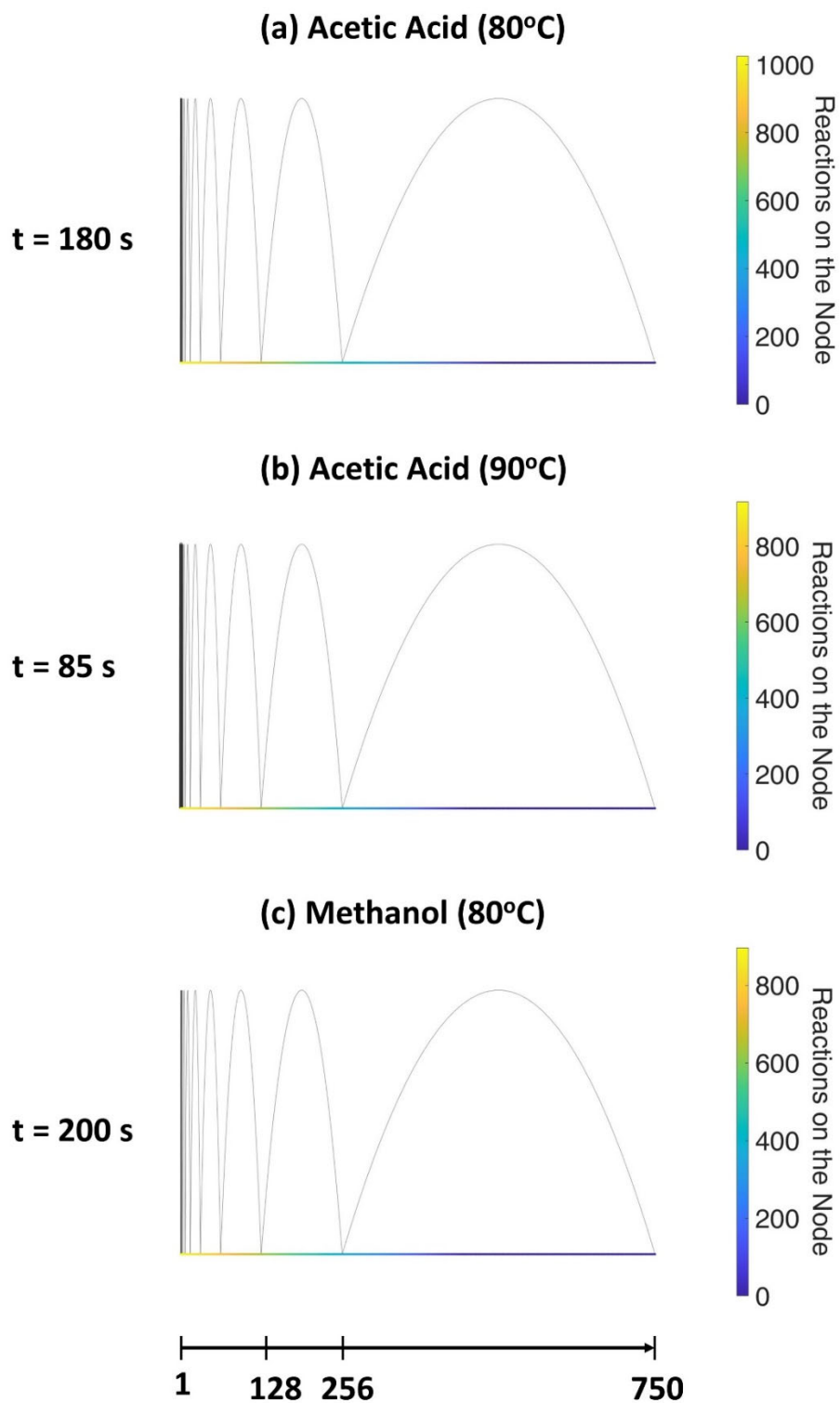


Figure S11: Most dominant pathway of nuclei formation as a function of operating conditions at the onset of nucleation. The number line scale shown at the bottom applies to all plots in the figure.

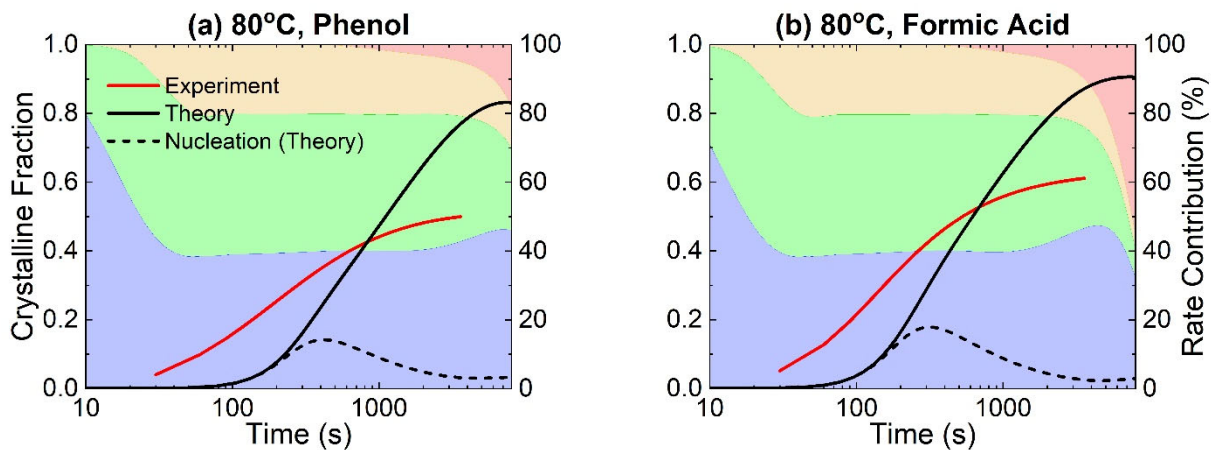


Figure S12: Theoretical and experimental crystalline fraction and relative rate contributions for (a) phenol and (b) formic acid as catalysts.

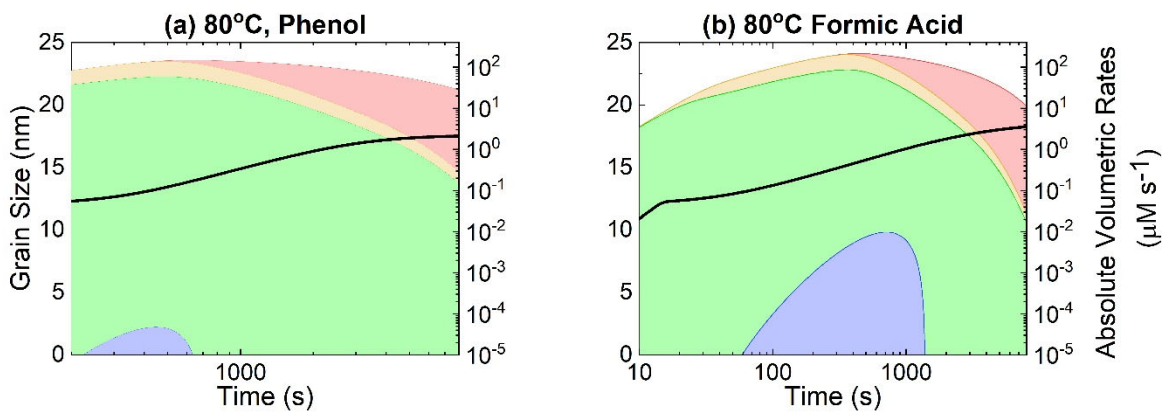


Figure S13: Theoretical and experimental grain size and absolute volumetric rates for (a) phenol and (b) formic acid as catalysts.

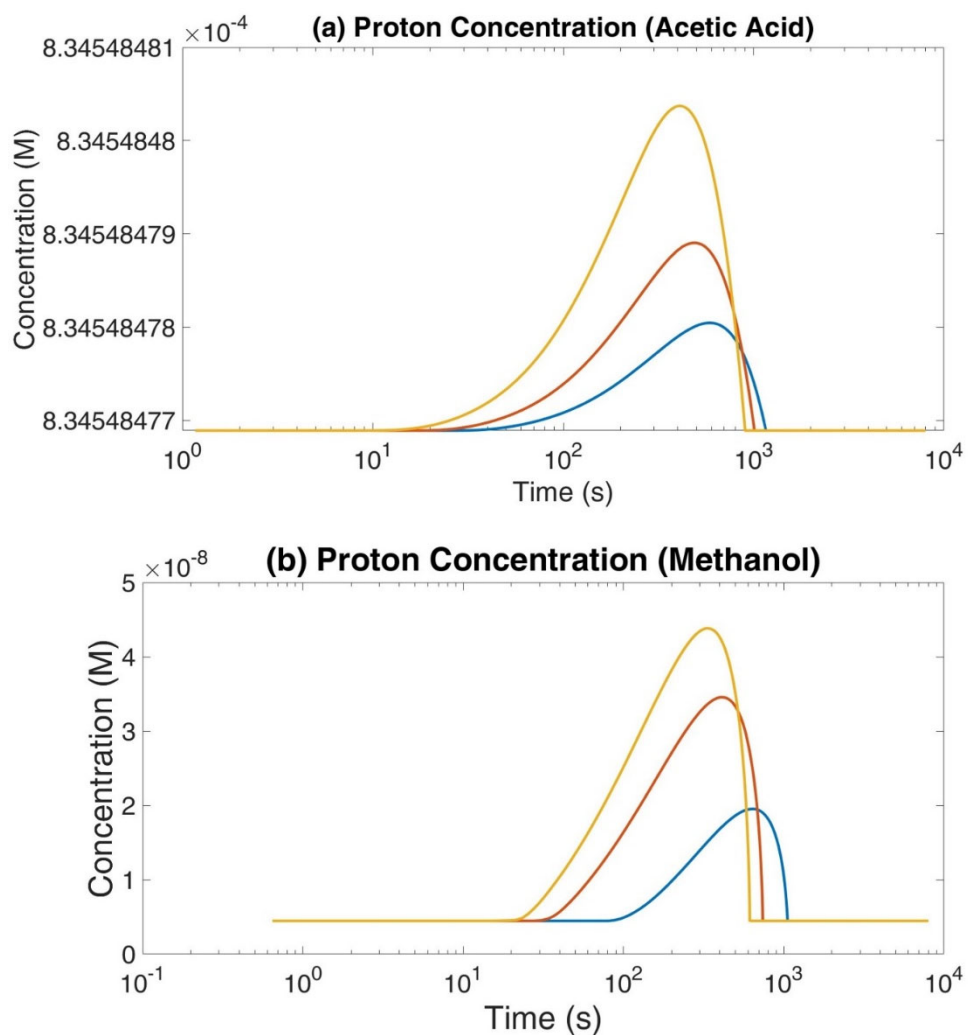


Figure S14: Concentration of proton in the solution as a function of time and temperatures for (a) acetic acid catalyst and (b) methanol catalyst. In both plots, the blue line represents 80°C , the red line represents 85°C , and the yellow line represents 90°C .

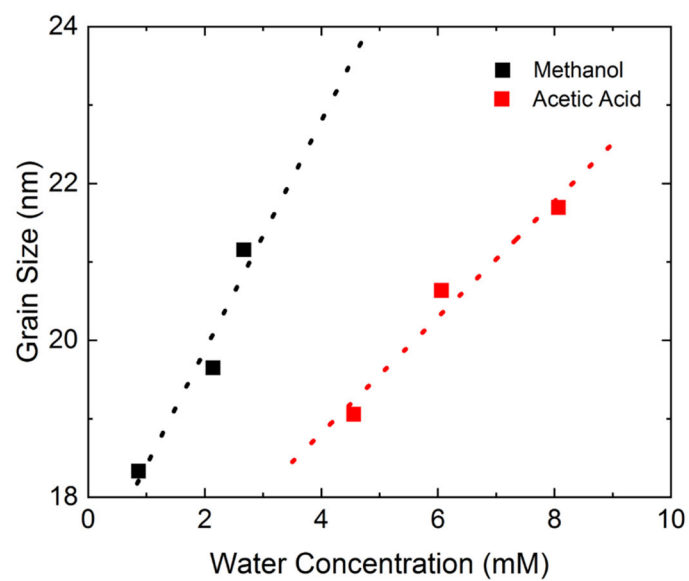


Figure S15: Steady state grain size at varying temperatures as a function of water concentration in the system. Obtained results are comparable to previously observed phenomena of effect of water on grain size.

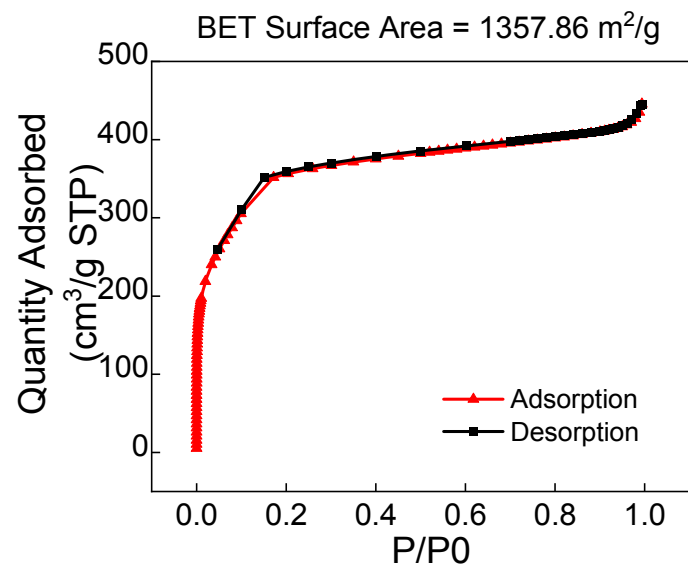


Figure S16: N₂ adsorption isotherm for BET surface area analysis of COF-5.

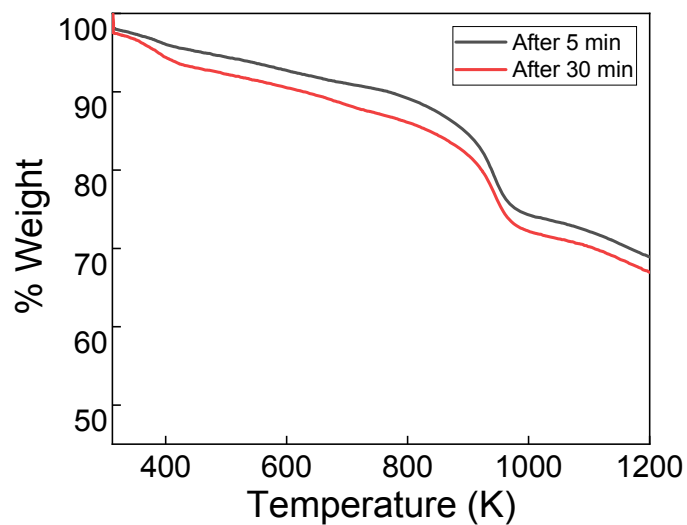


Figure S17: Thermogravimetric analysis (TGA) of as synthesized COF-5 samples obtained after 5 min and 30 min of synthesis at $T=80^{\circ}\text{C}$ and 40mM acetic acid added as catalyst. The molar concentration of precursors was maintained at 3:2(PBBA:HHTP). The powder was filtered and thoroughly washed once with acetone and vacuum dried.

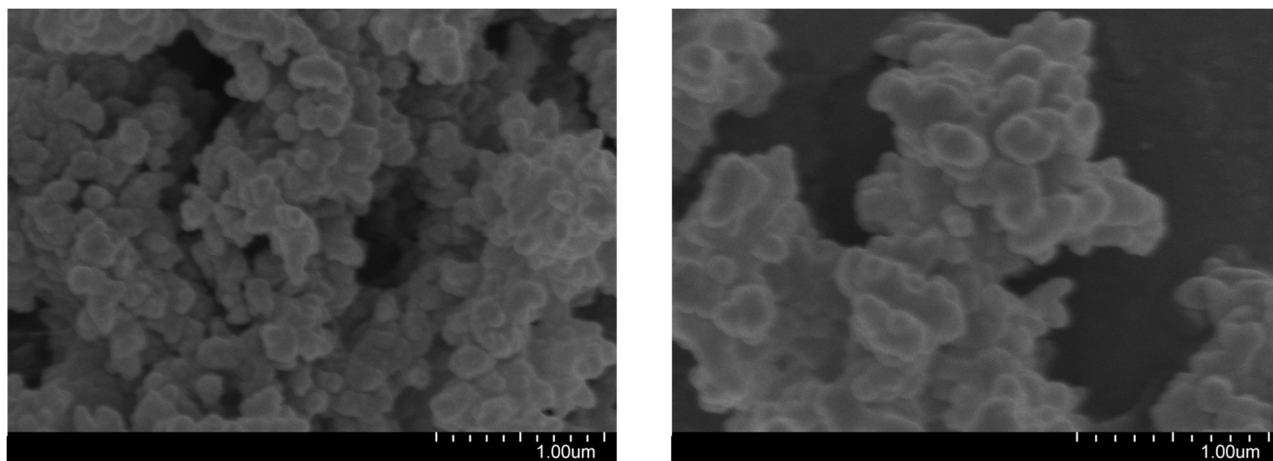


Figure S18: SEM images of COF-5 samples obtained after 5 min (left) and 30 min (right) of synthesis at $T=80^{\circ}\text{C}$ and 40mM acetic acid added as catalyst. The molar concentration of precursors was maintained at 3:2(PBBA:HHTP). The powder was filtered and thoroughly washed once with acetone and vacuum dried.

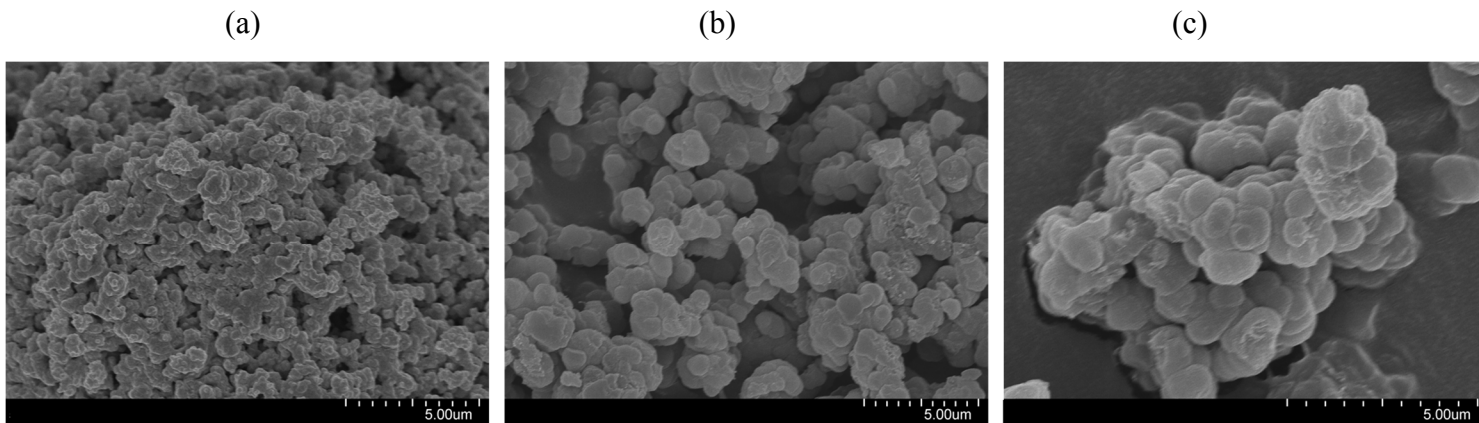
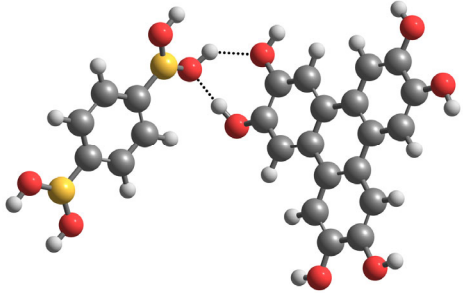
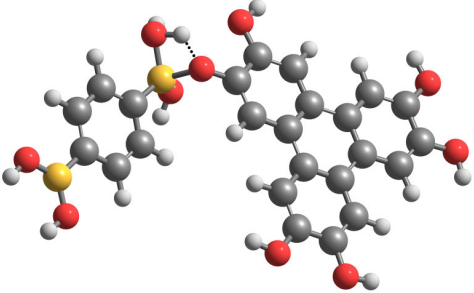
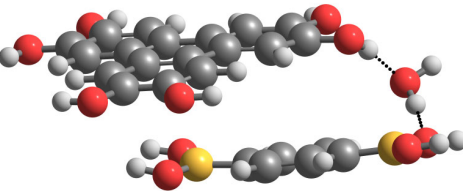
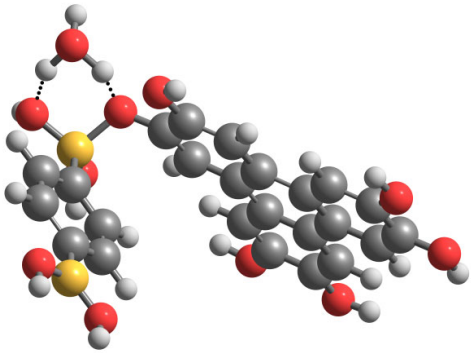
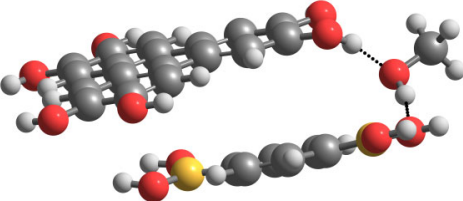
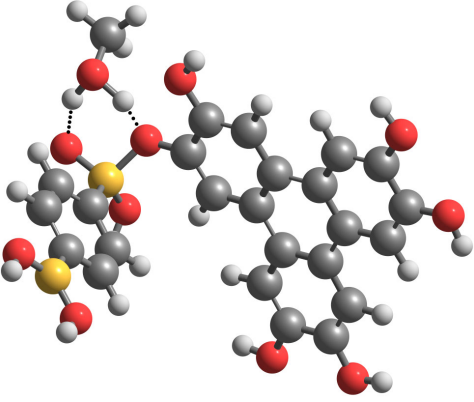


Figure S19: SEM images of COF-5 samples from three separate experiments with synthesis conditions: $T=80^{\circ}\text{C}$ and 40mM acetic acid added as catalyst. In case of (a) No water was added, (b) 10mM water was added and, (c) 20mM water was added. The reaction was allowed to run for 24 hours and the powder was filtered and washed thoroughly with acetone. The powder was vacuum dried and studied under SEM.

Table S1: Reactant and transition state structures of HHTP and PBBA in presence of different catalysts.

Catalyst	Reactant	Transition state
Without catalyst		
Water		
Methanol		

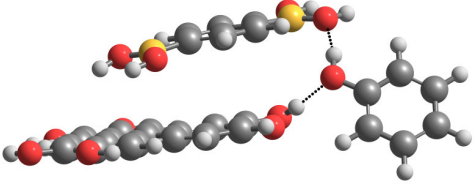
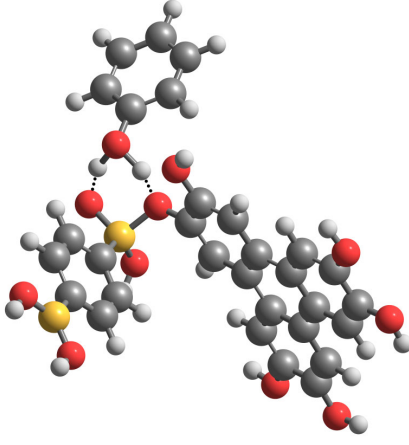
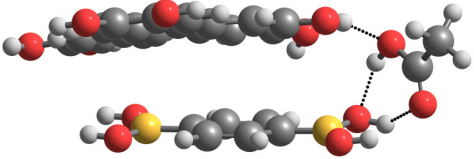
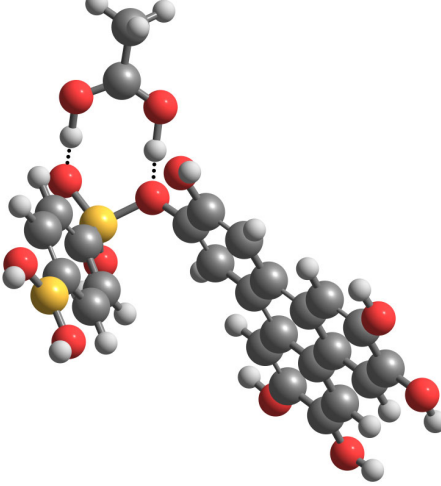
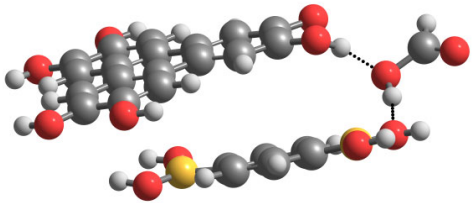
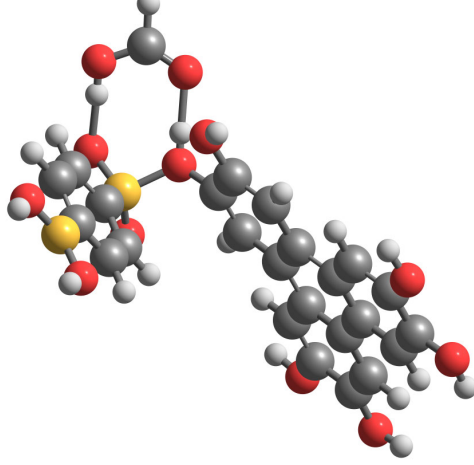
Catalyst	Reactant	Transition state
Phenol		
Acetic acid		
Formic acid		

Table S2: Transition state free energy barriers.

Reaction condition	ΔG^\ddagger , Kcal/mol
No catalyst	25.97
Water	16.84
Methanol	16.08
Phenol	20.93
Acetic acid	13.49
Formic acid	13.90

Table S3: Values of standard deviations over three reproducible runs for all temperatures and catalyst conditions in experimental crystal fraction.

Catalyst	Temperature	Average SD (%)
Acetic Acid	80	2.35
	85	1.65
	90	1
Methanol	80	3.03
	85	4.65
	90	4.85

Table S4: Details of the experimental conditions used in the article and role in the microkinetic model.

#	Initial Concentration of HHTP (mM)	Initial Concentration of PBBA (mM)	Temperature (° C)	Catalyst	Used for
1	12	8	80	Acetic Acid	Calculation of volume of active catalytic sites per unit concentration using error minimization of initiation rate constant
2	12	8	85	Acetic Acid	Calculation of volume of active catalytic sites per unit concentration using error minimization of initiation rate constant
3	12	8	90	Acetic Acid	Prediction
4	12	8	80	Methanol	Error minimization of initiation, hydrolysis, aggregation, water evaporation rate constants
5	12	8	85	Methanol	Error minimization of initiation, hydrolysis, aggregation, water evaporation rate constants
6	12	8	90	Methanol	Prediction
7	12	8	80	Phenol	Calculation of volume of active catalytic sites per unit concentration using error minimization of initiation rate constant

8	12	8	80	Formic acid	Calculation of volume of active catalytic sites per unit concentration using error minimization of initiation rate constant
---	----	---	----	-------------	---

Table S5: Values of the error minimized parameters.

Parameter	Temperature (° C)	Value	Units
k'_f	80	0.081	$L mol^{-1} s^{-1}$
k'_f	85	0.1018	$L mol^{-1} s^{-1}$
k_b	80	0.021	$L^2 mol^{-2} s^{-1}$
k_a	80	603	$L mol^{-1} s^{-1}$
$k_{evap,w}$	80	8×10^{-6}	$mol L^{-1} s^{-1}$
k_b	85	0.038	$L^2 mol^{-2} s^{-1}$
k_a	85	963	$L mol^{-1} s^{-1}$
$k_{evap,w}$	85	1.1×10^{-5}	$mol L^{-1} s^{-1}$
γ	80	-0.0412	Dimensionless
γ	85	-0.0246	Dimensionless

Table S6: Standard deviation for the XRD grain size.

Catalyst	Temperature (°C)	Average Standard Deviation (nm)
Methanol	80	0.723
Methanol	85	0.84
Methanol	90	1.1
Acetic Acid	80	0.77
Acetic Acid	85	0.89
Acetic Acid	90	1.4

Table S7: Value of fitted parameters for nucleation and growth kernels.

Catalyst	Parameter	Value
Acetic Acid	$k_{0,n}$	4.5464×10^{-5}
Acetic Acid	A_n	0.6862
Acetic Acid	B_n	4.096
Acetic Acid	$k_{0,g}$	5.0236×10^{10}
Acetic Acid	A_g	0.01773
Acetic Acid	B_g	1.067
Methanol	$k_{0,n}$	1.2392×10^6
Methanol	A_n	0.5657
Methanol	B_n	3.704
Methanol	$k_{0,g}$	8.0976×10^{11}
Methanol	A_g	0.02243
Methanol	B_g	1.063

Table S8: Summary of various growth phases and the corresponding governing process and a conceptual schematic.

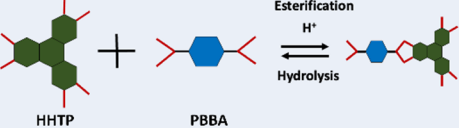
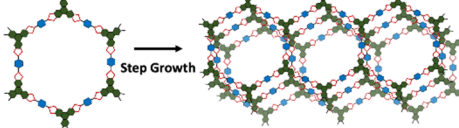
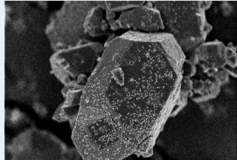
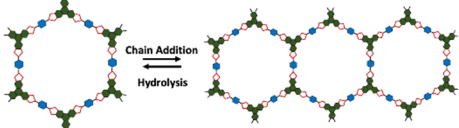
Growth Phase	Governing Processes	Schematic
Esterification Reaction	Acid Catalyzed Initiation Reaction	 <p>HHTP + PBBA $\xrightleftharpoons[H^+]{\text{Esterification}}$ [Linked Structure] $\xrightleftharpoons{\text{Hydrolysis}}$ HHTP + PBBA</p>
Exponential Growth	Step reaction	 <p>Step Growth</p>
Transition	Onset of termination reaction due to surface stabilization	
Stationary	Full termination followed by chain reaction	 <p>Chain Addition \rightleftharpoons Hydrolysis</p>

Table S9: Comparison of experimentally obtained kinetics with previously published work

Features	COF-5 reaction kinetics (published)(9, 11, 12)	COF-5 reaction kinetics (This work)	Comments/Justification
Chemistry of the initiation reaction	Role of solvent composition optimized to improve the initial rate of the COF-5 formation	Identified the role of additives as catalysts and related their catalytic activity to their buffering capacity	This work adds to the understanding of the solvent environment for the synthesis of COF-5
Stoichiometry and the reaction order	The formation of COF-5 from reactants is considered with limited understanding of nucleation and growth phases. COF-5 formation is believed to follow non-elementary reaction kinetics.	Considered the entire reaction network to understand the nucleation and growth dynamics. The initiation reaction is elementary as we identify the stoichiometry and the smallest growth unit from the crystal structure and subsequently study the evolution of the smallest SBU in a comprehensive step-by-step manner.	Non-elementary reaction published considered one single reaction for quantitative analysis and hypothesized multiple step formation of COFs. This work validates this hypothesized schematic quantitatively and provides additional insights on alternate reaction pathways involving multiple steps (initiation, aggregation and termination) for COF-5 formation.
Nucleation and growth mechanisms	It is proposed that monomer addition and templated growth govern COF-5 growth without a side-by-side experimental-theoretical approach.	Quantitatively determined the role of each step in the contribution to COF-5 nucleation and growth	Refer to Figure 3 and Figure 4 of the main manuscript.
Rate constants and activation energies	Activation energies: 92-113 kJ/mol (based on initial rates). Only reported for methanol catalyst	Along with overall activation energies obtained experimentally, the microkinetic model provides the individual nucleation and growth activations for reactions involving methanol and acidic catalysts introduced in this work.	Refer to Figures 5e and 5f of the main manuscript. The experimental rates and activation values match with the previously published work that utilized methanol as a catalyst.
Reversibility of the reactions	The role of water on the crystal domain size, however, limited mechanistic understanding was depicted	Identified the role of water as (1) proton donor and (2) responsible for hydrolysis of the COF-5 crystals. Water dynamics and evolution of water as the reaction proceeds are quantified	Refer to Figure 4 of the main manuscript and Figure S15 of the SI.
Optimization of catalyst and identification of limiting rate constant	Not studied previously	Identified the limiting rate constant and lowest possible activation barrier for COF-5 synthesis (Figure 5e)	This article adds to the understanding of COF-5 synthesis.

Table S10: Comparison of reaction model of this work with previously published work

Property	Previous Work(13, 14)	This work
Initiation	Simple Non-elementary initiation reaction	Acid-Catalyzed Esterification reaction that allows calculation of limiting rate constant
Reversibility of the reaction	Not considered at all	Considered, and absolute volumetric rates were found (Figure 4)
Monomer addition and oriented attachment	Considered	The similar approach considered as that of previous work
Evaporation	Not considered	It is considered, and the activation barriers were reported in Figure 5e of the main manuscript

References

1. M. e. Frisch *et al.* (2016) Gaussian 16. (Gaussian, Inc. Wallingford, CT).
2. J.-D. Chai, M. Head-Gordon, Long-range corrected hybrid density functionals with damped atom–atom dispersion corrections. *Physical Chemistry Chemical Physics* **10**, 6615-6620 (2008).
3. W. J. Hehre, R. Ditchfield, J. A. Pople, Self—consistent molecular orbital methods. XII. Further extensions of Gaussian—type basis sets for use in molecular orbital studies of organic molecules. *The Journal of Chemical Physics* **56**, 2257-2261 (1972).
4. C. Peng, H. Bernhard Schlegel, Combining synchronous transit and quasi-newton methods to find transition states. *Israel Journal of Chemistry* **33**, 449-454 (1993).
5. C. Peng, P. Y. Ayala, H. B. Schlegel, M. J. Frisch, Using redundant internal coordinates to optimize equilibrium geometries and transition states. *J Comput Chem* **17**, 49-56 (1996).
6. K. Fukui, The path of chemical reactions—the IRC approach. *Accounts of chemical research* **14**, 363-368 (1981).
7. B. J. Smith *et al.*, Colloidal Covalent Organic Frameworks. *ACS Cent Sci* **3**, 58-65 (2017).
8. R. L. Laurence, R. Galvan, M. V. Tirrell, "Mathematical modelling of polymerization kinetics" in *Polymer Reactor Engineering*, C. McGreavy, Ed. (Springer Netherlands, Dordrecht, 1994), 10.1007/978-94-011-1338-0_3 chap. Chapter 3, pp. 87-124.
9. A. P. Cote *et al.*, Porous, crystalline, covalent organic frameworks. *Science* **310**, 1166-1170 (2005).
10. A. V. Bandura, S. N. Lvov, The Ionization Constant of Water over Wide Ranges of Temperature and Density. *Journal of Physical and Chemical Reference Data* **35**, 15-30 (2006).
11. B. J. Smith, W. R. Dichtel, Mechanistic studies of two-dimensional covalent organic frameworks rapidly polymerized from initially homogenous conditions. *J Am Chem Soc* **136**, 8783-8789 (2014).
12. H. Li *et al.*, Nucleation and Growth of Covalent Organic Frameworks from Solution: The Example of COF-5. *J Am Chem Soc* **139**, 16310-16318 (2017).
13. A. V. Dighe *et al.*, Autocatalysis and Oriented Attachment Direct the Synthesis of a Metal-Organic Framework. *JACS Au* **2**, 453-462 (2022).
14. A. V. Dighe, R. Y. Nemade, M. R. Singh, Modeling and Simulation of Crystallization of Metal–Organic Frameworks. *Processes* **7**, 11 (2019).